

RhFe Alloying Promotes the Efficient and Selective Conversion of Syngas to Ethanol

Wei Zhou,^[a] Scott R. Docherty,^[a] Erwin Lam,^[b] Christian Ehinger,^[a] Xiaoyu Zhou,^[a]
Yuhui Hou,^[b] Paco Laveille,^[b] and Christophe Copéret*^[a]

[a]Department of Chemistry and Applied Bioscience, ETH Zürich, CH-8093 Zürich, Switzerland

[b]Swiss Cat+ East, ETH Zürich, CH-8093 Zürich, Switzerland

*Corresponding author: ccoperet@inorg.chem.ethz.ch

Abstract: The direct conversion of syngas to ethanol is a promising route for the sustainable production of value-added chemicals and fuels. While Fe-promoted Rh-based catalysts have long been studied because of their notable activity and selectivity towards ethanol, the nature of Rh-Fe interaction and the catalyst structure under reaction conditions remain poorly understood due to the intrinsic complexity of heterogeneous catalysts prepared by conventional approaches. In this work, we construct well-defined RhFe@SiO₂ model catalysts via surface organometallic chemistry (SOMC), composed of small and narrowly distributed nanoparticles supported on silica. Such RhFe@SiO₂ catalyst converts syngas into ethanol, reaching an overall selectivity of 38% ethanol among all products at 8.4% CO conversion, while the non-promoted Rh@SiO₂ catalyst mostly yields methane (selectivity > 90%) and no ethanol. Detailed *in situ* XAS and DRIFTS studies reveal that the RhFe@SiO₂ catalyst corresponds to an Rh-Fe alloy with ca. 3:1 Rh/Fe ratio alongside residual Fe^{II} single site. The alloy is stable under working conditions, promoting high activity and ethanol selectivity.

Keywords: syngas conversion; ethanol; Fe promoted Rh-based catalysts; SOMC approach; *In situ* XAS

Introduction

Syngas (CO/H₂) serves as a crucial platform for transforming the non-petroleum carbon resources, such as coal, natural gas, shale gas and biomass, into liquid fuels and basic chemicals.^[1-3] In that context, major efforts have focused on the direct conversion of syngas into ethanol, an ideal fuel additive, promising hydrogen carrier, and versatile building-block in chemical synthesis.^[4-8] Among potential candidates, Rh-based catalysts show promising ethanol selectivity in syngas conversion in the presence of specific additives, so-called promoters.^[9-12] Among them, Fe has been shown to be particularly efficient to trigger ethanol production of Rh-based catalysts.^[9, 13-17] However, the promotional effect of Fe under syngas conversion conditions remains poorly understood, partly because of the ill-defined catalyst structures resulting from conventional synthetic approaches. For example, there are ongoing debates regarding whether the RhFe alloy or Rh-FeO_x interfaces are crucial for promoting ethanol synthesis.^[13, 14, 16, 17]

In that context, Surface organometallic chemistry (SOMC) has emerged as a powerful synthetic methodology to generate tailored catalysts and to interrogate the role of composition and interfaces.^[18-20] Specifically, SOMC exploits the surface termination of oxide supports, especially surface OH groups, M_S-OH, to anchor well-defined metal precursors, L_nMX_x through protonolysis, generating atomically dispersed surface species, M_S-O-ML_nX_{x-1} (ca. 1 site/nm²) while releasing HX. Subsequent thermal treatment under vacuum or reactive atmospheres like H₂ can yield isolated metal sites or nanoparticles with tailored compositions or interfaces. Overall, SOMC generates well-defined models of heterogeneous catalysts, where each component can be selectively introduced and their state probed through detailed characterization. Taken together with catalytic studies and detailed *in situ* or *operando* spectroscopic investigations, molecular-level structure-activity relationships and guideline principles can be elaborated, thus providing opportunities for rational catalyst development. Our group has successfully implemented this approach to explore and understand various heterogeneous catalysts used for propane dehydrogenation,^[21,22] selective oxidation of methane^[23] and CO₂ hydrogenation.^[20,24,25]

Considering the unique ability of Fe to promote the formation of ethanol with Rh-based

catalysts, here we have thus decided to interrogate the promotional role of Fe in syngas conversion, employing SOMC to prepare well-defined RhFe@SiO₂ model catalysts. We find that the introduction of Fe dramatically enhances the activity in syngas conversion and shifts the product selectivity from almost pure methane to ethanol, along with some amount of methanol. Detailed *in situ* XAS and DRIFTS studies demonstrate the formation of RhFe alloyed nanoparticles dispersed on a silica decorated with Fe(II) single sites, avoiding the presence of bulk FeO_x or Fe carbides. Both *in situ* XAS and DRIFTS studies show that the RhFe alloy remains stable under reaction, which is crucial in improving both catalyst activity and ethanol selectivity.

Results and discussion

First, Rh is dispersed via grafting on the residual surface silanols of a silica decorated with isolated Fe^{II}, prepared from the reaction of Fe₂(OSi(OtBu)₃)₄ on partially dehydroxylated at 700 °C (SiO₂₋₇₀₀) followed by a thermal treatment under vacuum.^[26] This tailored support, denoted Fe^{II}@SiO₂ and containing ca. 0.9 Fe^{II} nm⁻² (Figure S1), displays an IR spectrum free of organic ligands, with isolated –OH groups (Figure S2). Upon reaction of Rh(COD)(DIA), a recently developed molecular precursor amenable for grafting,^[27] the –OH stretch at 3747 cm⁻¹ disappears (Figure 1a), and the resulting material, coined Rh^I-Fe^{II}@SiO₂, displays peaks at ca. 3250 cm⁻¹ (N-H stretching), 3100-2700 cm⁻¹ (C-H stretching), 1700-1600 cm⁻¹ (C=N and C=C stretching) and 1500-1300 cm⁻¹ (C-H bending) in the IR spectrum (Figure 1b). These results confirm that the Rh(COD)(DIA) grafts via protonolysis with surface silanols. Subsequent reduction under H₂ at 400 °C yields a black solid, RhFe@SiO₂, containing the regenerated Si-OH group but no organic residue. A monometallic Rh@SiO₂ is prepared by the same approach using SiO₂₋₇₀₀ as previously reported.^[27]

Transmission electron microscopy (TEM) shows that RhFe@SiO₂ contains highly-dispersed and small nanoparticles with a narrow particle size distribution (1.6 ± 0.5 nm, Figure 1c). The particle sizes of RhFe@SiO₂ are notably smaller than for the corresponding Rh@SiO₂ (3.3 nm), prepared via the same approach, already indicating a strong interaction between Rh and Fe (Table S1). The absence of diffraction peaks in RhFe@SiO₂ is consistent with the observation of reduced particle size in TEM, while metallic Rh is detected in Rh@SiO₂ (Figure

S3). FTIR spectra of adsorbed CO shows that two peaks at around 2070 cm^{-1} and 1890 cm^{-1} are both observed over RhFe@SiO_2 and Rh@SiO_2 (Figure 1d); they are assigned to linearly bound CO and bridging CO adsorbed on metallic Rh, respectively. Note that the peak at around 2070 cm^{-1} is significantly broader for RhFe@SiO_2 than for Rh@SiO_2 , potentially indicating alloying upon H_2 treatment (*vide infra*).

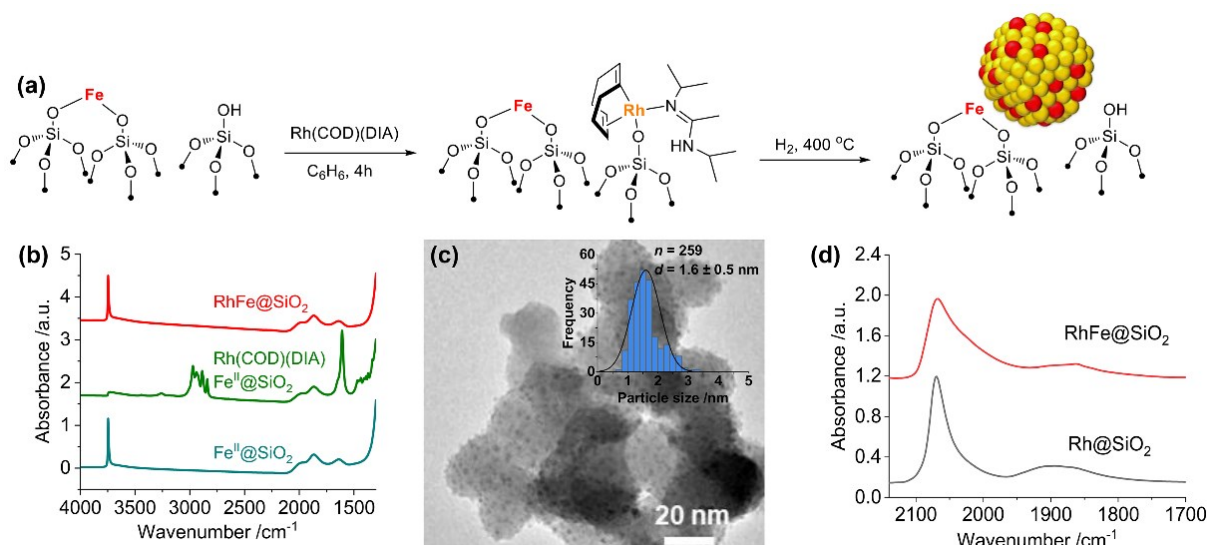


Figure 1. (a) Schematic procedure for grafting of $\text{Rh}(\text{COD})(\text{DIA})$ on $\text{Fe}^{\text{II}}@/\text{SiO}_2$ followed by reduction under H_2 at $400\text{ }^\circ\text{C}$. (b) IR spectra throughout the synthesis of RhFe@SiO_2 starting from the second grafting. (c) Particle size distribution and TEM images of RhFe@SiO_2 (d) FTIR spectra of CO adsorbed on Rh@SiO_2 (black line) and RhFe@SiO_2 (red line) under 2.5 mbar CO pressure at room temperature.

The as-prepared RhFe@SiO_2 and Rh@SiO_2 catalysts are next evaluated for syngas conversion at 25 bar ($\text{H}_2/\text{CO}/\text{N}_2 = 2:1:1.5$). Following exposure to air, the catalysts are reduced at $400\text{ }^\circ\text{C}$ under H_2 prior to evaluating their performances in syngas conversion. By altering the gas flow rate while fixing the temperature at $250\text{ }^\circ\text{C}$, the RhFe@SiO_2 catalyst provides a high selectivity to $\text{CH}_3\text{CH}_2\text{OH}$ ($> 33\%$) over a wide range of CO conversion (Figure 2a), along with some amount of CH_3OH (around 25%). Notably, the CH_4 and CH_3OH selectivities decrease with increasing CO conversion, while the opposite trend is observed for ethanol, indicating that C-C coupling is more favorable at longer contact time and ethanol is likely a secondary product. Moreover, study on the effect of temperature indicates that the ethanol selectivity can be

slightly increased with increasing in CO conversion, while sacrificing some CH₃OH selectivity. Overall, an ethanol selectivity of up to 38% at 8.4% CO conversion can be obtained at 270 °C (Figure 2b). In contrast, under various conditions, Rh@SiO₂ invariably shows inferior CO conversion (< 1%) and high selectivity (> 90%) along with small amounts of C₂-C₄ hydrocarbons and no oxygenate organic products (Figure S4 and S5), consistent with previous reports related to non-promoted Rh catalyst for syngas conversion. [16, 28, 29] Note that the catalytic activity of the support – Fe^{II}@SiO₂ – for syngas conversion is below detection limit under identical conditions. These findings suggest that the synergy between Rh and Fe is crucial for promoting ethanol formation in syngas conversion.

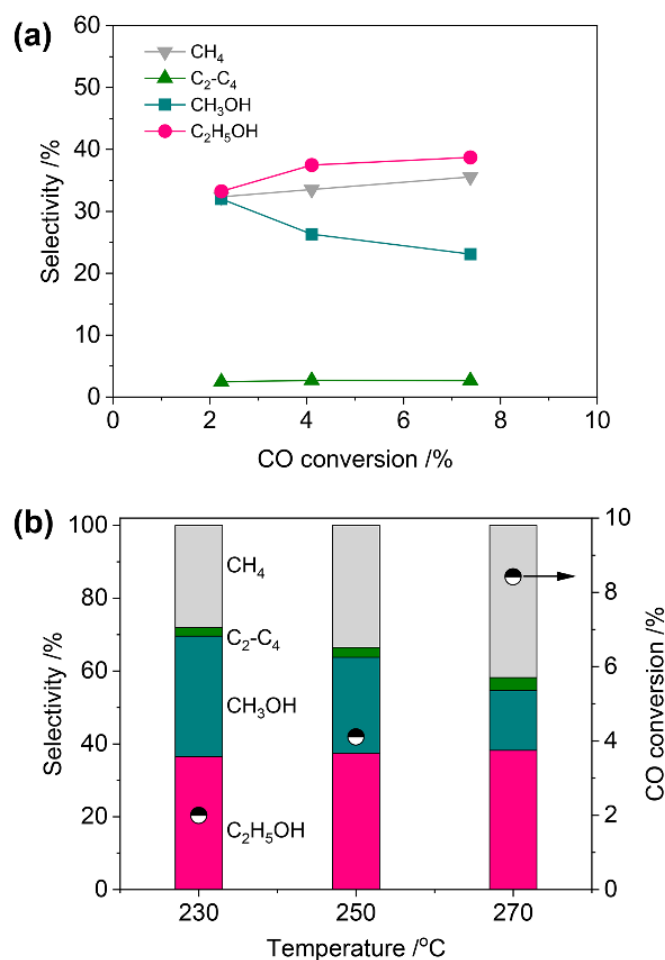


Figure 2. (a) Product selectivity vs CO conversion over RhFe@SiO₂ catalyst for syngas conversion. Reaction conditions: $W_{\text{cat}} = 50$ mg, CO/H₂/N₂ = 1:2:1.5, $F = 2-8$ mL/min, $T = 250$ °C, $P = 25$ bar. (b) The effect of temperature on RhFe@SiO₂ catalysts. Reaction conditions: $W_{\text{cat}} = 50$ mg, CO/H₂/N₂ = 1:2:1.5, $F = 4$ mL/min, $T = 230-270$ °C, $P = 25$ bar.

In order to understand the origin of the promotional effect of Fe, we next carried out *in situ* X-ray Absorption Spectroscopy (XAS) experiments to study the structure evolution of RhFe@SiO₂ under different conditions at both the Rh and Fe K-edges (Figure S6). The evolution of structure is first analyzed from Rh K-edge (Figure 3a and 3b), and the fitted values are shown in Figure S7-S10 and summarized in Table S2. The Rh K-edge X-ray absorption near-edge structure (XANES) spectrum of air-exposed RhFe@SiO₂ bears some resemblance to Rh₂O₃ reference (Figure 3a). Simultaneously, two peaks at ~ 1.5 Å and ~ 2.4 Å are observed in the Fourier transform of EXAFS spectra, which are attributed to Rh-O and Rh-Rh scattering path based on the references (Figure 3b). The fitting results reveal that the coordination number (CN) of Rh-Rh and Rh-O are 4.8 and 2.7, respectively (Figure S8 and Table S2). These results suggest that the RhFe@SiO₂ catalyst contains both oxidized and metallic Rh species after exposure to air, which is quite different from what is observed for the monometallic Rh@SiO₂ exposed to air, since it contains exclusively metallic Rh (Table S2).^[27]

Next *in situ* X-ray adsorption near-edge structure (XANES) at Rh K-edge are collected to monitor the evolution of air-exposed RhFe@SiO₂ during the H₂ temperature programmed reduction (H₂-TPR) process. The spectra are analyzed using linear combination fitting (LCF) to identify the different Rh species present in the sample. Note that the Rh@SiO₂ is used as the standard Rh metal spectra to minimize the effect of particle size on the XANES spectra (Figure S11). As shown in Figures 3c and 3d, LCF analysis indicates that the air-exposed RhFe@SiO₂ sample can be described as a mixture of ca. 40% Rh₂O₃ and 60% Rh metal. The XANES spectra evolve towards metallic Rh during H₂-TPR, suggesting that the oxidized Rh species in the air-exposed RhFe@SiO₂ can be reversibly reduced. Overall, after H₂ reduction at 400 °C, while the peak at ~ 1.5 Å observed in the Fourier transformed EXAFS spectra vanishes (Figure 3b), consistent with the XANES results. The fitting result of EXAFS spectrum show an average CN of 6.8 and 1.7 for Rh-Rh and Rh-Fe respectively (Figure S9 and Table S2), implying the formation of Rh-Fe alloy after H₂ reduction.^[16, 30] Wavelet transform (WT) analyses shows a maximum intensity near 9 Å⁻¹ and 2.4 Å and a weaker intensity near 5 Å⁻¹ and 1.5 Å for air-exposed catalysts, while a maximum intensity near 9 Å⁻¹ and 2.4 Å and a weaker intensity near 7 Å⁻¹ and 1.9 Å are observed for post H₂ reduction, further indicative of alloy formation (Figure 3e).

Notably, no change is observed for the XANES during the course of syngas conversion. The fitting of post-syngas EXAFS spectrum indicates similar CN compared to the reduced catalyst (Figure 3a, 3b, Figure S9, S10 and Table S2). Moreover, the wavelet transform (WT) analyses of post-syngas and reduced catalysts are rather similar (Figure 3e). These findings reveal that alloying persists throughout CO hydrogenation. For the monometallic Rh@SiO₂, it exclusively remains metallic throughout CO hydrogenation (Figure S13 and Table S2), which is well-known for methanation catalysts in syngas conversion.^[9]

In situ Fe K-edge XAS spectra under the same conditions are also collected and analyzed to gain more insights into the interplay between Rh and Fe. As shown in Figure S14a, compared to Fe^{II}@SiO₂, the edge position of air-exposed RhFe@SiO₂ shifts to higher position. The intensity of the pre-edge peak at ca. 7113 eV, corresponding to the transition from 1s to 3d-like levels, increases to some extent due to a greater amount of 4p mixing with 3d orbitals when Fe^{II} is oxidized to Fe^{III}.^[31] Moreover, the first derivative spectra of air-exposed catalyst significantly shift to higher energy compared to the Fe^{II}@SiO₂ reference (Figure S14b). These results clearly demonstrate that the pristine Fe^{II} was oxidized to Fe^{III} under air-exposed condition. Furthermore, fitting of EXAFS spectrum only shows an average CN of 4.8 for Fe-O scattering contribution in the air-exposed catalyst (Figure S14c, Figure S15, and Table S3).

During H₂-TPR, the intensity of pre-edge gradually decreases and the edge position gradually shifts to a lower energy (Figure S18). These indicate that the oxidized Fe species was reversibly reduced. After H₂ reduction at 400 °C, LCF analysis of the Fe K edge XANES spectrum using Fe^{II}@SiO₂ and Fe foil as references demonstrates that ca. 77% Fe is in the state of Fe^{II}@SiO₂, while the remaining 23% Fe is reduced to Fe⁰ and is incorporated into the Rh nanoparticle to form the Rh-Fe alloy as discussed above with a Rh/Fe⁰ ratio of 3.3:1 (Figure S19, Table S4). Moreover, a new peak at 2.3 Å in R space emerges, which is 0.2 Å higher than that of Fe-Fe scattering path, indicating the absence of Fe aggregation (Figure S14c). The EXAFS fitting results show that this peak belongs to the Fe-Rh scattering path with an average CN of 0.5, which is in accordance with the results from Rh K-edge (Figure S16 and Table S3). Similar to what is observed from Rh K-edge, no changes are observed at the Fe K-edge during syngas conversion (Figure S14, Figure S17, S20, and Table S3). Therefore, considering the syngas conversion results, it is proposed that the unique structure of RhFe alloy supported over

$\text{Fe}^{\text{II}}@ \text{SiO}_2$, that persists under catalytic condition, is crucial for shifting the products from CH_4 to $\text{CH}_3\text{CH}_2\text{OH}$.

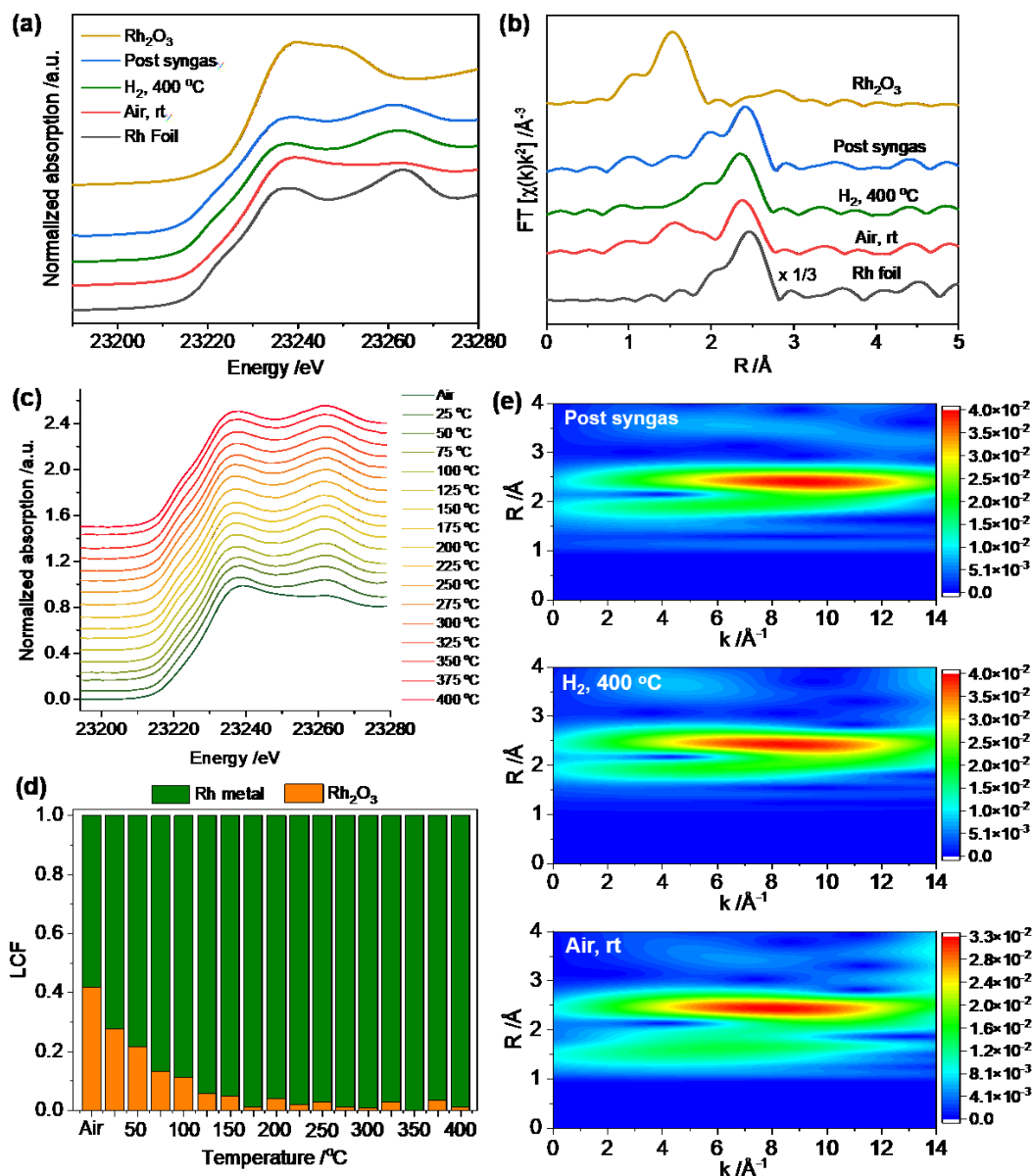


Figure 3. *In situ* XAS of $\text{RhFe}@ \text{SiO}_2$ at Rh K-edge under different conditions: (a) XANES spectra; (b) the k^2 -weighted Fourier transforms of EXAFS spectra; (c) *In situ* XANES collected during H_2 temperature programmed reduction. (d) Results of linear combination fitting (LCF) of Rh K-edge XANES. (e) Wavelet transform analysis of Rh K-edge EXAFS data.

In situ Diffuse Reflectance Infrared Fourier Transform Spectroscopy (DRIFTS) measurements are next undertaken to gain insights about possible reaction intermediates formed under CO hydrogenation. When exposed to a gas mixture of CO/H₂/Ar (2:1:1) at 250 °C, Rh@SiO₂ shows IR bands at 2063 and 1918 cm⁻¹, attributed to linearly- and bridge-bonded CO*, respectively (Figure 4a).^[32, 33] In addition, adsorbed CH_x* species (bands at 2985 and 2935 cm⁻¹) and gaseous CH₄ (band at 3015 cm⁻¹) are also observed. Similar species can also be observed with RhFe@SiO₂: CO* bands at 2059 and 1909 cm⁻¹, CH_x* bands at 2983, 2937 and 2856 cm⁻¹ along with gaseous CH₄ (bands centered at 3015 cm⁻¹), albeit with lower intensities for linearly- and bridge-bonded CO*. These findings imply that Fe decreases CO chemisorption, likely explaining the enhanced activity in CO hydrogenation considering that CO is as a poison.^[34] The significant decrease of the bridge-bonded CO* intensity also indicates that the RhFe alloys persist under CO hydrogenation conditions, further supporting XAS analysis.

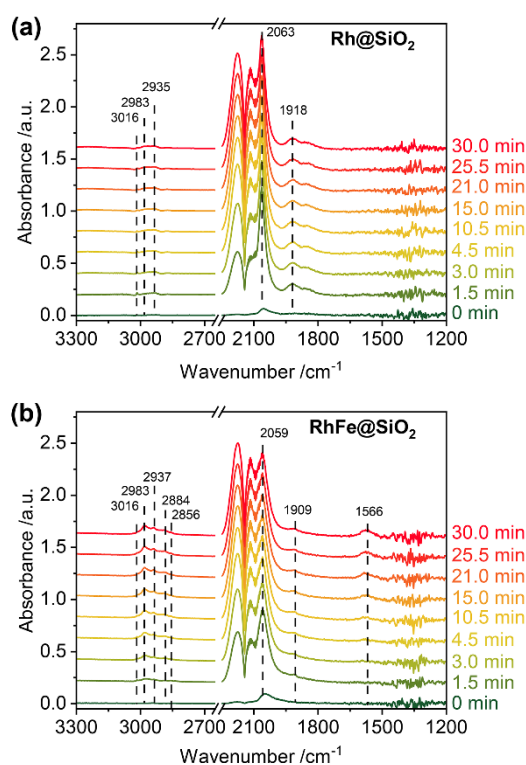


Figure 4. (a) *In situ* DRIFTS spectra on Rh@SiO₂ (a) and RhFe@SiO₂ collected under CO/H₂/Ar (1:2:1) at 250 °C.

In addition, the intensity of the bands associated with CH_x^* species is significantly higher with RhFe@SiO_2 , while the intensity of bands associated with gaseous CH_4 is lower (Figure S21), suggesting that the presence of Fe enables the accumulation of CH_x species and suppresses the hydrogenation of CH_x species into CH_4 . The accumulation of CH_x species over surface of RhFe@SiO_2 catalyst parallels the observed rise in C-C coupling products, as revealed by the increase ethanol selectivity and productivity.^[9, 34, 35] Furthermore, additional IR bands, assigned to formate species and likely associated with methanol formation, are also observed at 2884 and 1566 cm^{-1} over RhFe@SiO_2 .^[36, 37] Overall, the alloying of Fe with Rh enables to decrease the amount of adsorbed CO^* , while promoting the formation of specific reaction intermediates, e.g. adsorbed CH_x and formates, improving the selectivity and productivity in oxygenates products, in particular ethanol, while suppressing methanation.

In summary, well-defined RhFe@SiO_2 catalysts prepared via SOMC shows that Fe promotes the dramatic increase in activity in syngas conversion and shifts the selectivity of Rh from methane to ethanol. *In situ* XAS experiments demonstrate that ca. 20% fraction of the overall Fe is incorporated into Rh nanoparticles after H_2 reduction, to form Rh-Fe alloy nanoparticles with an Rh/Fe ratio of 3.3:1, along with residual Fe^{II} isolated sites dispersed on SiO_2 . This structure is maintained during syngas conversion, and all data show that the formation of stable RhFe alloyed nanoparticles is probably key to increasing the activity and shifting the selectivity of Rh from methane to high ethanol productivity. The formation of stable alloys is key to this observed reactivity switch and provide insights to design more efficient catalysts for the conversion of syngas to ethanol. Overall, this study illustrates that the combination of SOMC and advanced *in situ* spectroscopy is a powerful tool to develop structure-performance relationship at molecular level.

Acknowledgements

This publication was created as part of NCCR Catalysis (grant number 180544), a National Center of Competence in Research funded by the Swiss National Science Foundation. C.C. and S.R.D. acknowledge the Swiss National Science Foundation (grants 200021_169134, and 200020B_192050), while C.E. acknowledges the Swiss National Science Foundation (grant

200020B_192050) and the Scholarship Fund of the Swiss Chemical Industry (SSCI). Dr. W. V. Beek and Dr. D. Stoian at the Swiss Norwegian Beamlines (SNBL, ESRF) are acknowledged for the provision of beamtime and support with *in situ* XAS experiments via proposal A31-1-168 and A31-1-222. Furthermore, ScopeM is gratefully acknowledged for their support and assistance in this work through project No. 2460 and 2658.

Conflict of interest

The authors declare no conflict of interest.

References:

- [1] W. Zhou, K. Cheng, J. Kang, C. Zhou, V. Subramanian, Q. Zhang, Y. Wang, *Chem. Soc. Rev.* **2019**, *48*, 3193-3228.
- [2] X. Pan, F. Jiao, D. Miao, X. Bao, *Chem. Rev.* **2021**, *121*, 6588-6609.
- [3] K. T. Rommens, M. Saeys, *Chem. Rev.* **2023**, *123*, 5798-5858.
- [4] G. Prieto, S. Beijer, M. L. Smith, M. He, Y. Au, Z. Wang, D. A. Bruce, K. P. de Jong, J. J. Spivey, P. E. de Jongh, *Angew. Chem. Int. Ed.* **2014**, *53*, 6397-6401.
- [5] W. Zhou, J. Kang, K. Cheng, S. He, J. Shi, C. Zhou, Q. Zhang, J. Chen, L. Peng, M. Chen, Y. Wang, *Angew. Chem. Int. Ed.* **2018**, *57*, 12012-12016.
- [6] J. Kang, S. He, W. Zhou, Z. Shen, Y. Li, M. Chen, Q. Zhang, Y. Wang, *Nat. Commun.* **2020**, *11*, 827.
- [7] T. Lin, X. Qi, X. Wang, L. Xia, C. Wang, F. Yu, H. Wang, S. Li, L. Zhong, Y. Sun, *Angew. Chem. Int. Ed.* **2019**, *58*, 4627-4631.
- [8] H. Yue, X. Ma, J. Gong, *Acc. Chem. Res.* **2014**, *47*, 1483-1492.
- [9] H. T. Luk, C. Mondelli, D. C. Ferré, J. A. Stewart, J. Pérez-Ramírez, *Chem. Soc. Rev.* **2017**, *46*, 1358-1426.
- [10] G. Liu, G. Yang, X. Peng, J. Wu, N. Tsubaki, *Chem. Soc. Rev.* **2022**, *51*, 5606-5659.
- [11] C. Wang, J. Zhang, G. Qin, L. Wang, E. Zuidema, Q. Yang, S. Dang, C. Yang, J. Xiao, X. Meng, C. Mesters, F.-S. Xiao, *Chem* **2020**, *6*, 646-657.
- [12] X. Pan, Z. Fan, W. Chen, Y. Ding, H. Luo, X. Bao, *Nat. Mater.* **2007**, *6*, 507-511.

- [13] S. S. Nathan, A. S. Asundi, A. S. Hoffman, J. Hong, C. Zhou, F. D. Vila, M. Cargnello, S. R. Bare, S. F. Bent, *J. Catal.* **2022**, *414*, 125-136.
- [14] P. Preikschas, M. Plodinec, J. Bauer, R. Kraehnert, R. Naumann d'Alnoncourt, R. Schlögl, M. Driess, F. Rosowski, *ACS Catal.* **2021**, *11*, 4047-4060.
- [15] N. Yang, A. J. Medford, X. Liu, F. Studt, T. Bligaard, S. F. Bent, J. K. Norskov, *J. Am. Chem. Soc.* **2016**, *138*, 3705-3714.
- [16] R. M. Palomino, J. W. Magee, J. Llorca, S. D. Senanayake, M. G. White, *J. Catal.* **2015**, *329*, 87-94.
- [17] X. Huang, D. Teschner, M. Dimitrakopoulou, A. Fedorov, B. Frank, R. Kraehnert, F. Rosowski, H. Kaiser, S. Schunk, C. Kuretschka, R. Schlogl, M. G. Willinger, A. Trunschke, *Angew. Chem. Int. Ed.* **2019**, *58*, 8709-8713.
- [18] C. Coperet, A. Comas-Vives, M. P. Conley, D. P. Estes, A. Fedorov, V. Mougel, H. Nagae, F. Nunez-Zarur, P. A. Zhizhko, *Chem. Rev.* **2016**, *116*, 323-421.
- [19] M. K. Samantaray, V. D Elia, E. Pump, L. Falivene, M. Hard, S. O. Chikh, L. Cavallo, J.-M. Basset, *Chem. Rev.* **2020**, *120*, 734-813.
- [20] S. R. Docherty, C. Copéret, *J. Am. Chem. Soc.* **2021**, *143*, 6767-6780.
- [21] S. R. Docherty, L. Rochlitz, P.-A. Payard, C. Copéret, *Chem. Soc. Rev.* **2021**, *50*, 5806-5822.
- [22] L. Rochlitz, Q. Pessemesse, J. W. A. Fischer, D. Klose, A. H. Clark, M. Plodinec, G. Jeschke, P.-A. Payard, C. Copéret, *J. Am. Chem. Soc.* **2022**, *144*, 13384-13393.
- [23] J. Meyet, A. Ashuiev, G. Noh, M. A. Newton, D. Klose, K. Searles, A. P. van Bavel, A. D. Horton, G. Jeschke, J. A. van Bokhoven, C. Copéret, *Angew. Chem. Int. Ed.* **2021**, *60*, 16200-16207.
- [24] E. Lam, K. Larmier, P. Wolf, S. Tada, O. V. Safonova, C. Copéret, *J. Am. Chem. Soc.* **2018**, *140*, 10530-10535.
- [25] S. R. Docherty, O. V. Safonova, C. Coperet, *J. Am. Chem. Soc.* **2023**, *145*, 13526-13530.
- [26] P. Sot, M. A. Newton, D. Baabe, M. D. Walter, A. P. van Bavel, A. D. Horton, C. Coperet, J. A. van Bokhoven, *Chem. Eur. J.* **2020**, *26*, 8012-8016.
- [27] W. Zhou, S. R. Docherty, C. Ehinger, X. Zhou, C. Copéret, *Chem. Sci.* **2023**, *14*, 5379-5385.
- [28] F. Xue, W. Chen, X. Song, X. Cheng, Y. Ding, *RSC Adv.* **2016**, *6*, 35348-35353.
- [29] J. Wang, Q. Zhang, Y. Wang, *Catal. Today* **2011**, *171*, 257-265
- [30] M. Ichikawa, T. Fukushima, *J. Phys. Chem.* **1986**, *90*, 1222-1224.

- [31] T. E. Westre, P. Kennepohl, J. G. DeWitt, B. Hedman, K. O. Hodgson, E. I. Solomon, *J. Am. Chem. Soc.* **1997**, *119*, 6297-6314.
- [32] A. Egbebi, V. Schwartz, S. H. Overbury, J. J. Spivey, *Catal. Today* **2010**, *149*, 91-97.
- [33] J. A. Chudek, M. W. McQuire, G. W. McQuire, C. H. Rochester, *J. Chem. Soc. Faraday Trans.* **1994**, *90*, 3699-3709.
- [34] Y. Choi, P. Liu, *J. Am. Chem. Soc.* **2009**, *131*, 13054-13061.
- [35] R. L. Arevalo, H. Nakanishi, *Catal. Lett.* **2024**, *154*, 3418-3425.
- [36] Y. Wang, S. Kattel, W. Gao, K. Li, P. Liu, J. G. Chen and H. Wang, *Nat. Commun.* **2019**, *10*, 1166.
- [37] V. Lochar, *Appl. Catal. A:Gen.* **2006**, *309*, 33-36.

Entry for the Table of Contents

